Journal of
Mechanics of
Materials and Structures

ACCURATE SIMULATION OF MIXED-MODE COHESIVE CRACK PROPAGATION IN QUASI-BRITTLE STRUCTURES USING EXACT ASYMPTOTIC FIELDS IN XFEM: AN OVERVIEW

Bhushan Lal Karihaloo and Qi-Zhi Xiao

Volume 6, No. 1-4 January–June 2011

mathematical sciences publishers

JOURNAL OF MECHANICS OF MATERIALS AND STRUCTURES
Vol. 6, No. 1-4, 2011

ACCURATE SIMULATION OF MIXED-MODE COHESIVE CRACK PROPAGATION IN QUASI-BRITTLE STRUCTURES USING EXACT ASYMPTOTIC FIELDS IN XFEM: AN OVERVIEW

BHUSHAN LAL KARIHALOO AND QI-ZHI XIAO

The extended finite element (XFEM) enriches the standard local FE approximations with known information about the problem, with the use of the partition of unity. This allows the use of meshes that do not conform to a discontinuity and avoids adaptive re-meshing as the discontinuity grows as required with the conventional FEM. When the crack tip asymptotic field is available and used as the enrichment function, XFEM is more accurate than FEM allowing the use of a much coarser mesh around the crack tip. Such asymptotic fields have been known for a long time for traction-free cracks (the Williams expansions) but have only recently been derived for cohesive cracks (Karihaloo–Xiao expansions). In this paper an overview of latter expansions is given for a range of cohesive laws and their usefulness in the simulation of cohesive crack propagation is demonstrated on two examples of concrete and fibre-reinforced concrete flexural members.

1. Introduction

The cohesive zone (or crack) model of Hillerborg et al. [1976] has been extensively used in the study of localization and failure in quasi-brittle materials (such as concrete and fibre-reinforced concrete) and structures. Borst et al. [2004] have given a concise overview of the various ways for the numerical implementation of the cohesive zone methodology.

The knowledge of the asymptotic crack tip displacement fields is especially useful in the recently developed extended finite element methodology (XFEM) (see [Moës et al. 1999; Strouboulis et al. 2001; Babuška et al. 2003; Karihaloo and Xiao 2003], for example). XFEM enriches the standard local FE approximations with known information about the problem, with the use of the partition of unity (PU). It avoids meshes conforming with the discontinuity and adaptive re-meshing as the discontinuity grows as is the case with the FEM. In [Karihaloo and Xiao 2003] we demonstrated that for a crack with traction-free faces, when the crack tip asymptotic field is available and used as enrichment function, XFEM not only avoids using a mesh conforming with the crack but is also more accurate than FEM. Hence XFEM can use a much coarser mesh around the crack tip. However, when the enrichment function differs from the true asymptotic crack tip field, the mesh needs to be refined in the same manner as in the FEM. Thus it is necessary to know the true asymptotic displacement field around a cohesive crack tip in order to exploit fully the advantages of XFEM.

The application of XFEM to the simulation of the growth of cohesive cracks in quasi-brittle materials has received considerable attention. However, adjacent to the cohesive crack tip, the enrichment function is chosen as the jump function [Wells and Sluys 2001; Hansbo and Hansbo 2004; Zi and Belytschko 2003]

Keywords: Asymptotic displacement field, asymptotic stress field, cohesive crack, extended finite element (XFEM).

or a (branch) function which does not represent the true asymptotic nature of the displacement/stress field there [Moës and Belytschko 2002]. Since there is no singularity at the tip of a cohesive crack, a stress criterion is often used to judge the initiation and propagation of the crack. Therefore a reliable analysis of cohesive crack propagation requires an accurate knowledge of the crack tip field. However, although no singularity exists at the tip of a cohesive crack, the stresses obtained by direct differentiation of the displacements are not accurate, and cannot be used to predict accurately the growth of the tip, exactly as in the traction-free cracks.

In [Xiao and Karihaloo 2006a; Karihaloo and Xiao 2008; 2010] we have obtained universal asymptotic expansions at a cohesive crack tip, analogous to the Williams expansions at a traction-free crack tip for any normal cohesion-separation law (softening law) that can be expressed in a special polynomial with integer or fractional powers. This special form ensures that the radial and angular variations of the asymptotic fields are separable as in the Williams expansions. The coefficients of the expansions of course depend nonlinearly on the softening law and the boundary conditions. They demonstrated that many commonly used cohesion-separation laws, e.g., rectangular, linear, bilinear and exponential, can indeed be expressed very accurately in this special form. They also obtained universal asymptotic expansions when the cohesive crack faces are subjected to Coulomb friction. In [Liu et al. 2004; Xiao and Karihaloo 2006b; Xiao et al. 2007] we used this true crack tip asymptotic displacement field as a crack tip enrichment function in XFEM for the simulation of mode I cohesive crack propagation in quasi-brittle materials to improve the prediction of the stress field ahead of the cohesive crack even with a coarse mesh.

In cohesive cracks, the friction is considered for a finite opening. In this sense frictional cohesive cracks are different from the frictional contact of crack faces, where the crack faces are in contact and not open. However, in cohesive cracks, although the crack faces are not in contact because of the applied cohesive stresses, frictional forces can come into play between the faces when there is relative sliding. Many studies on the mixed mode cohesive cracks can also be found in the literature, but there is doubt about the accuracy of the cohesion-sliding relation because it is difficult to isolate it from frictional forces between the rough cohesive crack faces in quasi-brittle materials such as concrete.

In this paper, the Karihaloo–Xiao asymptotic expansions are reviewed for a range of cohesive laws and their usefulness in the simulation of cohesive crack propagation by XFEM is demonstrated on two examples of concrete and fibre-reinforced concrete flexural members.

This paper is organised as follows: Section 2 gives cohesive laws of concrete and fibre-reinforced concrete suitable for the asymptotic analysis of cohesive cracks; Section 3 gives a brief overview of the mathematical formulation and boundary conditions and of the asymptotic fields for several cases; Section 4 discusses the implementation of the asymptotic fields in XFEM. Two illustrative examples of concrete and fibre-reinforced concrete flexural members are given and discussed in Section 5.

2. Cohesive laws for concrete and fibre-reinforced concrete

Cornelissen et al. [1986] introduced the following exponential relation to fit their results from uniaxial tests on double edge notched normal and lightweight concrete panels:

$$\frac{\sigma}{f_t} = f\left(\frac{w}{w_c}\right) - \frac{w}{w_c} f(1), \qquad f\left(\frac{w}{w_c}\right) = \left[1 + \left(C_1 \frac{w}{w_c}\right)^3\right] e^{-C_2 w/w_c} \tag{1}$$

It fits their experimental results with a high degree of accuracy. In (1), σ and f_t are the stress normal to the cohesive crack face and the uniaxial tensile strength, respectively; w and w_c are the opening displacement of the cohesive crack faces, and the critical opening displacement of the pre-existing macrocrack tip at which the cohesive crack tip begins to grow; and C_1 and C_2 are fitting parameters. Details of the test set up as well as the cohesive relation (1) can be found in [Karihaloo 1995]. Other widely used softening laws for concrete are the linear relation

$$\hat{\sigma} = 1 - \hat{w}, \tag{2}$$

the bilinear relation

$$\hat{\sigma}_y = \begin{cases} 1 - (1 - \hat{f}_1)\dfrac{\hat{w}}{\hat{w}_1} & \text{if } 0 \le \hat{\sigma}_y \le \hat{f}_1, \\ \dfrac{\hat{f}_1}{1-\hat{w}_1}(1 - \hat{w}) & \text{if } \hat{f}_1 < \hat{\sigma}_y \le 1, \end{cases} \tag{3}$$

and the power-law relationship

$$\hat{\sigma}_y^m + \hat{w}^{2m} = 1. \tag{4}$$

In (2)–(4) we have $\hat{\sigma}_y = \sigma_y/f_t$, $\hat{w} = w/w_c$, $\hat{f}_1 = f_1/f_t$, $\hat{w}_1 = w_1/w_c$, and m ranges from 0.20 to 0.27 for different concrete grades. Moreover, the two linear parts of (3) can be rewritten into two linear laws. The first part can be written into (2) using a new definition of w_c as

$$w_c = \frac{w_1}{1 - \hat{f}_1}. \tag{5}$$

The second part can be written into (2) using a new definition of f_t as

$$f_t = \frac{f_1}{1 - \hat{w}_1}. \tag{6}$$

We shall also consider two further cohesion-separation laws not commonly associated with concrete, namely

$$\hat{\sigma}_y = 1 \tag{7}$$

and

$$\hat{\sigma}_y = 1 - \hat{w}^{2(L+1)}, \quad L = 1, 2, 3, \ldots. \tag{8}$$

The cohesion-separation law (7) is akin to the Dugdale [1960] model of plasticity in thin metallic sheets, which is also frequently used in fibre-reinforced polymeric materials, whereas the law (8) is commonly used in studying the fracture process zone embedded within the large plastic zone in metals.

For the high-performance fibre-reinforced concrete CARDIFRC [Benson and Karihaloo 2005], tensile tests showed that the post-peak cohesion-separation curve can be accurately represented by the polynomial

$$\hat{\sigma}_y = 116.76\hat{w}^7 - 468.08\hat{w}^6 + 738.12\hat{w}^5 - 612.10\hat{w}^4 + 272.71\hat{w}^3 - 59.33\hat{w}^2 + 2.89\hat{w} + 1, \tag{9}$$

in which $f_t = 16\,\text{MPa}$ and $w_c = 6.5\,\text{mm}$.

In [Xiao and Karihaloo 2006a] we showed that the polynomial

$$\hat{\sigma}_y = 1 + \sum_{i=1}^{L} \alpha_i \hat{w}^{(2/3)i} - \left(1 + \sum_{i=1}^{L} \alpha_i\right) \hat{w}^{(2/3)(L+1)} \tag{10}$$

not only fits the experimental results of Cornelissen et al. (Equation (1) above), but also many commonly used cohesion-separation laws, including the rectangular (7), linear (2), and bilinear (3).

The choice of the special form of the cohesion-separation relation (10) involving as it does fractional powers of $\hat{w}$ may seem strange but it ensures that the asymptotic fields at the cohesive crack tip are separable into radial and angular variations exactly as Williams expansions at a traction-free crack tip.

In [Karihaloo and Xiao 2008] we showed that separable asymptotic crack tip fields are also obtainable for the following cohesion-separation relation not involving fractional powers of $\hat{w}$:

$$\hat{\sigma}_y = 1 + \sum_{i=1}^{L} \alpha_i \hat{w}^{2i} - \left(1 + \sum_{i=1}^{L} \alpha_i\right) \hat{w}^{2(L+1)}, \tag{11}$$

where L is an integer.

3. Mathematical formulation

The mathematical formulation is fully described in [Karihaloo and Xiao 2008], so that only a very brief overview will suffice here. For plane problems, the stresses and displacements in the Cartesian coordinate system centred at the cohesive crack tip can be expressed in terms of two analytic functions $\phi(z)$ and $\chi(z)$ of the complex variable $z = re^{i\theta}$:

$$\begin{aligned} \sigma_x + \sigma_y &= 2\big[\phi'(z) + \overline{\phi'(z)}\big], \\ \sigma_x - \sigma_y + 2i\tau_{xy} &= 2\big[\bar{z}\phi''(z) + \chi''(z)\big], \\ 2\mu(u + iv) &= \kappa\phi(z) - z\overline{\phi'(z)} - \overline{\chi'(z)}, \end{aligned} \tag{12}$$

where a prime denotes differentiation with respect to z and an overbar the complex conjugate. In (12), $\mu = E/[2(1+\nu)]$ is the shear modulus; the Kolosov constant is $\kappa = 3 - 4\nu$ for plane strain or $\kappa = (3-\nu)/(1+\nu)$ for plane stress; E and ν are Young's modulus and Poisson's ratio, respectively.

For a general plane mixed mode I + II problem, the complex functions $\phi(z)$ and $\chi(z)$ can be chosen as series of complex eigenvalue Goursat functions

$$\phi(z) = \sum_{n=0} A_n z^{\lambda_n} = \sum_{n=0} A_n r^{\lambda_n} e^{i\lambda_n\theta}, \quad \chi(z) = \sum_{n=0} B_n z^{\lambda_n+1} = \sum_{n=0} B_n r^{\lambda_n+1} e^{i(\lambda_n+1)\theta}, \tag{13}$$

where the complex coefficients are $A_n = a_{1n} + ia_{2n}$ and $B_n = b_{1n} + ib_{2n}$. The eigenvalues λ_n and coefficients $a_{1n}, a_{2n}, b_{1n}, b_{2n}$ are real.

Substitution of the complex functions (13) into (12) gives the complete series expansions of the displacements and stresses near the tip of the crack. For details, see [Karihaloo and Xiao 2008].

These solutions need to satisfy the proper symmetry conditions along the line of extension ahead of the cohesive crack, and boundary conditions on the cohesive crack faces. Considering frictional cohesive crack faces, the boundary conditions on the cohesive crack ($0 = r = l_p$) are

$$\sigma_y|_{\theta=\pi} = \sigma_y|_{\theta=-\pi} \neq 0, \quad \tau_{xy}|_{\theta=\pi} = \tau_{xy}|_{\theta=-\pi} = -\mu\sigma_y|_{\theta=\pm\pi}, \tag{14}$$

where μ_f equals the positive or negative value of the coefficient of kinetic friction, which is assumed to be constant, depending on the relative sliding direction of the two crack faces. Specifically, $\mu_f > 0$ when the sliding displacement δ is positive and $\mu_f < 0$ when $\delta < 0$. The length of the process (cohesive) zone l_p is

either prescribed (i.e., an initial cohesive zone exists before the loading is applied, and does not propagate under the present loading) or is determined by the condition $\hat{w} = 1$ in the normal cohesion-separation relation (10) or (11) at the instant of growth of the pre-existing traction-free crack.

The separated crack tip asymptotic solutions can be obtained after satisfying the boundary conditions (14). The complete asymptotic solutions are composed of two parts, corresponding to integer ($\lambda_n = n+1$) and noninteger ($\lambda_n = (2n+3)/2$) eigenvalues, respectively. These solutions are given in [Karihaloo and Xiao 2008].

The displacements corresponding to the first integer eigenvalue are

$$\begin{aligned} 2\mu u &= r\{[a_{10}^I(\kappa-1)\cos\theta - 2\mu_f \sin\theta] - a_{20}^I(\kappa+1)\sin\theta - 2b_{10}^I(\cos\theta + \mu_f \sin\theta)\},\\ 2\mu v &= r\{[a_{10}^I(\kappa-1)\sin\theta + 2\mu_f \cos\theta] - a_{20}^I(\kappa+1)\cos\theta + 2b_{10}^I(\sin\theta - \mu_f \cos\theta)\}. \end{aligned} \tag{15}$$

The displacements corresponding to the second integer eigenvalue are

$$\begin{aligned} 2\mu u &= r^2\{a_{11}^I(\kappa\cos 2\theta - 2 - 3\mu_f \sin 2\theta) + a_{21}^I[-(\kappa+1)\sin 2\theta + 2] - 3b_{11}^I(\cos 2\theta + \mu_f \sin 2\theta)\},\\ 2\mu v &= r^2\{a_{11}^I(\kappa\sin 2\theta - 2 - 3\mu_f \cos 2\theta) + a_{21}^I[(\kappa+1)\cos 2\theta + 2] + 3b_{11}^I(\sin 2\theta - \mu_f \cos 2\theta)\}. \end{aligned} \tag{16}$$

The displacements corresponding to the first noninteger (fractional) eigenvalue are

$$\begin{aligned} 2\mu u &= r^{3/2}\{a_{10}^f[(\kappa+\tfrac{1}{2})\cos\tfrac{3}{2}\theta - \tfrac{3}{2}\cos\tfrac{1}{2}\theta] + a_{20}^f[-(\kappa+\tfrac{5}{2})\sin\tfrac{3}{2}\theta - \tfrac{3}{2}\sin\tfrac{1}{2}\theta]\},\\ 2\mu v &= r^{3/2}\{a_{10}^f[(\kappa-\tfrac{1}{2})\sin\tfrac{3}{2}\theta - \tfrac{3}{2}\sin\tfrac{1}{2}\theta] + a_{20}^f[(\kappa-\tfrac{5}{2})\cos\tfrac{3}{2}\theta + \tfrac{3}{2}\cos\tfrac{1}{2}\theta]\}. \end{aligned} \tag{17}$$

The displacements corresponding to the second noninteger eigenvalue are

$$\begin{aligned} 2\mu u &= r^{5/2}\{a_{11}^f[(\kappa+\tfrac{3}{2})\cos\tfrac{5}{2}\theta - \tfrac{5}{2}\cos\tfrac{1}{2}\theta] + a_{21}^f[-(\kappa+\tfrac{7}{2})\sin\tfrac{5}{2}\theta + \tfrac{5}{2}\sin\tfrac{1}{2}\theta]\},\\ 2\mu v &= r^{5/2}\{a_{11}^f[(\kappa-\tfrac{3}{2})\sin\tfrac{5}{2}\theta + \tfrac{5}{2}\sin\tfrac{1}{2}\theta] + a_{21}^f[(\kappa-\tfrac{7}{2})\cos\tfrac{5}{2}\theta + \tfrac{5}{2}\cos\tfrac{1}{2}\theta]\}. \end{aligned} \tag{18}$$

Here superscript I distinguishes coefficients associated with integer eigenvalues, whereas superscript f distinguishes coefficients associated with noninteger (fractional) eigenvalues.

For integer eigenvalues the opening displacement (COD) behind the cohesive zone tip and the sliding displacement of the cohesive crack faces vanish

$$w = v|_{\theta=\pi} - v|_{\theta=-\pi} = 0, \quad \delta = u|_{\theta=\pi} - u|_{\theta=-\pi} = 0, \tag{19}$$

while σ_y and τ_{xy} are nonzero along the cohesive crack faces with

$$\hat{\sigma}_y = \frac{\sigma_y}{f_t}\Big|_{\substack{\theta=\pm\pi \\ 0\le r\le l_p}} = \sum_{n=0} c_n r^n = 1 + \sum_{n=1} c_n r^n, \tag{20}$$

where

$$c_n = \frac{(n+1)(n+2)(a_{1n}^I + b_{1n}^I)\cos n\pi}{f_t} \tag{21}$$

with

$$c_0 = \frac{2(a_{10}^I + b_{10}^I)}{f_t}, \tag{22}$$

since $\sigma_y|_{\theta=\pm\pi} = f_t$ at $r = 0$.

For noninteger eigenvalues,

$$\sigma_y|_{\theta=\pm\pi} = 0, \tag{23}$$

$$\hat{w} = \frac{w}{w_c}\bigg|_{0\le r\le l_p} = \sum_{n=0} \bar{d}_n r^{(2n+3)/2} = \bar{d}_0 r^{3/2} + \sum_{n=1} \bar{d}_n r^{(2n+3)/2}, \tag{24}$$

$$\delta|_{0\le r\le l_p} = -\frac{\kappa+1}{\mu} \sum_{n=0} a^f_{2n} r^{(2n+3)/2} \sin\frac{2n+3}{2}\pi, \tag{25}$$

$$\bar{d}_n = \frac{\kappa+1}{\mu w_c} a^f_{1n} \sin\frac{2n+3}{2}\pi. \tag{26}$$

Set $d_0 = \bar{d}_0$ and $d_n = \bar{d}_n/d_0$ for $n \ge 1$. Then

$$d_0 = -\frac{\kappa+1}{\mu w_c} a^f_{10}, \quad d_n = -\frac{a^f_{1n}}{a^f_{10}} \sin\frac{2n+3}{2}\pi \tag{27}$$

By enforcing the cohesion-separation law (10) or (11), nonlinear relationships between d_n and c_n are obtained. The general relationships can be found in [12]. In [13], these general relationships have been explicitly derived for the simpler cohesion-separations laws (7) and (8).

4. Implementation in XFEM

To model the cohesive cracks in XFEM [Moës et al. 1999; Strouboulis et al. 2001; Babuška et al. 2003; Karihaloo and Xiao 2003], a standard local FE displacement approximation around the crack is enriched with discontinuous Heaviside functions along the crack faces behind the crack tip including the open traction-free part, and the crack tip asymptotic displacement fields at nodes surrounding the cohesive crack tip using the PU. The approximation of displacements for an element can be expressed in the form

$$\begin{Bmatrix} u^h(x) \\ v^h(x) \end{Bmatrix} = \sum_{i\in I} \phi_i(x) \begin{Bmatrix} u_{0i} \\ v_{0i} \end{Bmatrix} + \sum_{j\in J\cap I} \phi_j(x) H(x) \begin{Bmatrix} b_{1j} \\ b_{2j} \end{Bmatrix} + \sum_{m\in M_k\cap I} \phi_m(x) \begin{Bmatrix} u_m \\ v_m \end{Bmatrix}^{(\mathrm{tip},\kappa)}, \tag{28}$$

where I is the set of all nodes in the element, (u_{0i}, v_{0i}) are the regular degrees of freedom at node i, ϕ_i is the FE shape function associated with node i, J is the subset of nodes whose support is intersected by the crack but do not cover any cohesive crack tips, the function $H(x)$ is the Heaviside function centred on the crack discontinuity, and (b_{1j}, b_{2j}) are the corresponding additional degrees of freedom. M_k is the subset of nodes that are enriched around the cohesive crack tip k with the asymptotic displacements $u^{(\mathrm{tip},\kappa)}$ and $v^{(\mathrm{tip},\kappa)}$.

The general asymptotic field for each integer eigenvalue has three independent terms, e.g., (15)–(16), and each noninteger (fractional) eigenvalue has two independent terms, e.g., (17)–(18). The fields for integer and noninteger eigenvalues need to be used together to produce the crack opening and non-vanishing tractions.

In order to improve the accuracy of stresses, we may use eight terms corresponding to one noninteger eigenvalue and two integer eigenvalues as crack tip enrichment functions in (28)

$$\begin{Bmatrix} u \\ v \end{Bmatrix}^{(\text{tip})} = \boldsymbol{\Phi}(r,\theta)\boldsymbol{q}^{(\text{tip})} \tag{29}$$

where $\boldsymbol{q}^{(\text{tip})} = [a^I_{10}, a^I_{20}, b^I_{10}, a^f_{10}, a^f_{20}, a^I_{11}, a^I_{21}, b^I_{11}]^T$ are additional nodal degrees of freedom at the enriched nodes to be solved together with nodal displacements of conventional FEM.

In (29), $\boldsymbol{\Phi}$ is the matrix formed by (r, θ) terms dependent on the additional unknown coefficients in (15)–(18).

For a mode I frictionless cohesive crack, the leading asymptotic displacement terms which correspond to a first noninteger eigenvalue adopted in [Xiao and Karihaloo 2006a] that gives a normal displacement discontinuity over the cohesive-crack faces can be used as crack tip enrichment functions:

$$u = \frac{r^{3/2}}{2\mu} a_1[(\kappa + \tfrac{1}{2})\cos\tfrac{3}{2}\theta - \tfrac{3}{2}\cos\tfrac{1}{2}\theta], \tag{30}$$

$$v = \frac{r^{3/2}}{2\mu} a_1[(\kappa - \tfrac{1}{2})\sin\tfrac{3}{2}\theta - \tfrac{3}{2}\sin\tfrac{1}{2}\theta]. \tag{31}$$

There are two possible ways to implement the above expansions in the XFEM. The first is to consider directly the nonlinear relationships between d_n and c_n and to obtain the cohesive stresses from the expansions. This avoids iterations on the cohesion-separation law, but requires solution of a system of algebraic equations with nonlinear constraints. The second way is to treat c_n and d_n as independent variables, and satisfy the cohesion-separation law (10) or (11) iteratively. The cohesive stresses in this case are obtained from the cohesion-separation law but not the expansions. However, these expansions can be used to smooth the numerically computed results. This way is generally more convenient to implement [11-13], and will also be used in the two examples below.

5. Examples, results and discussion

In this section, we will analyze typical mode I cohesive cracking problems of plain and fibre-reinforced concrete using the above asymptotic fields and XFEM. We consider three-point bend beams without any initial crack (Figure 1, left) made of plain concrete with the constant softening law (7), and of CARDIFRC with the softening law (9). We actually assume a very small initial crack of length 0.1 mm at the bottom midpoint of the beam. A state of plane strain is considered for all specimens. The geometrical parameters are $l = 4b$, and $t = b$, where t is the specimen thickness in the out-of-plane direction. The x-direction of nodes with coordinates $(0, 0)$ and $(0, l)$ and y-direction of the node with coordinates $(b, l/2)$ are constrained; the central "point" load is distributed over two elements.

We consider first the three-point bend plain concrete beams with $b = 150$ mm. This problem was solved in [11] with XFEM using the enrichment functions (30) and (31) for the linear and bilinear cohesion separation relations (2) and (3). It was shown that very accurate results could be obtained in this way with a coarse mesh (Figure 1, right) that would have required a much finer mesh with conventional FEM.

We have re-analysed the three-point bend beam using the constant traction law (7) with

$$f_t = 3.14\,\text{MPa}, \quad w_c = 0.03886\,\text{mm}, \quad G_F = 122\,\text{N/m} \tag{32}$$

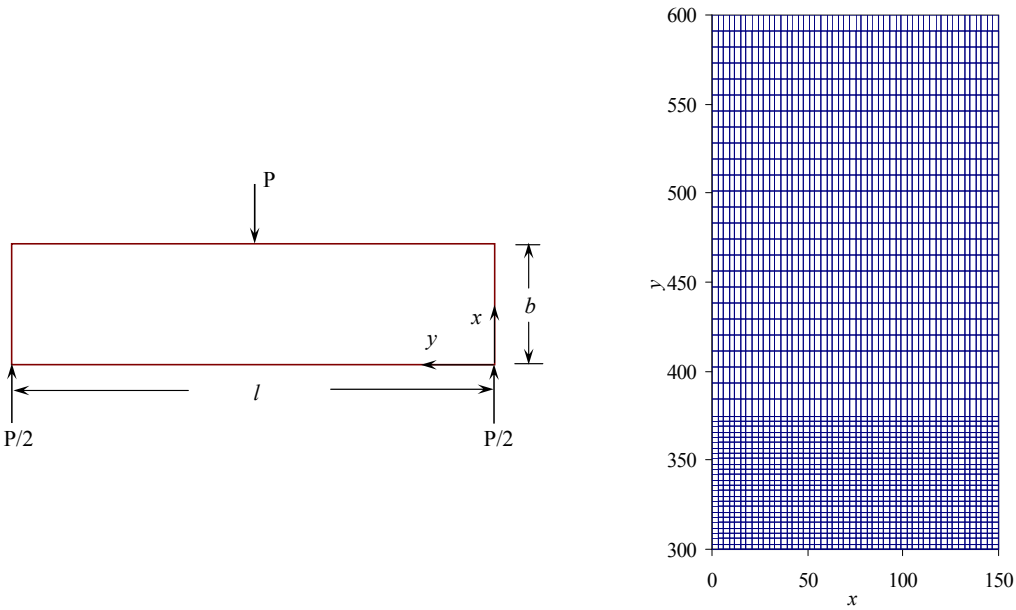

Figure 1. Left: three-point bend beam. Right: coarse mesh for one half of the specimen to the left of midspan (note rotation).

in order to study the influence of the shape of the cohesion-separation law on the global response. We have used the same coarse mesh as before (Figure 1, right). However to improve the accuracy further, we have used (15)–(18) as crack tip enrichment functions instead of the leading asymptotic displacement terms of a mode I frictionless cohesive crack (30) and (31) adopted in [Xiao and Karihaloo 2006a]. The nondimensional load-midspan deflection curve is shown in Figure 2 and compared with that of the bilinear law (*loc. cit.*). It is clear that although the tensile strength f_t and specific fracture energy G_F are the same, the initial branch of the cohesion-separation law produces very different responses: the constant traction law produces a higher peak load but a more brittle overall response with a significant snapback.

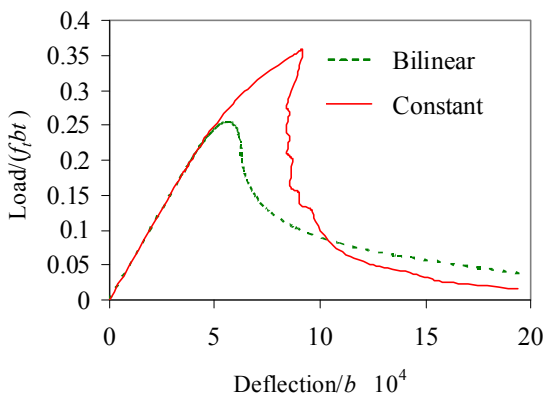

Figure 2. The nondimensional load-midspan deflection curves of the three-point bend beam with constant traction and bilinear softening laws.

Three-point bend fibre-reinforced concrete beam. We now consider a smaller three-point bend beam $b = 100\,\text{mm}$ made of CARDIFRC. We found it convenient to approximate the polynomial form of its cohesion separation relationship (9) by the bilinear relationship (3) with the material parameters $E = 48\,\text{GPa}$, $f_t = 16\,\text{MPa}$, $w_1 = 2.29\,\text{mm}$, $f_1 = 3.9088\,\text{MPa}$ and the Poisson's ratio ν equals 0.2. The constraint and loading conditions are identical to the plain concrete beam. The discretised mesh is also identical to that shown in Figure 1, right, after scaling the coordinates by a factor of $2/3$. The asymptotic displacements (30) and (31) are used as crack tip enrichment functions.

In the simulation, the first increment of the cohesive crack is 2.9 mm; thereafter the cohesive crack propagates by a segment of length 2 mm after each step. When the cohesive crack has developed over the entire depth of the specimen at a midspan deflection of about 3 mm, jump functions are used to enrich all nodes on the crack faces. The simulation is continued by increasing the deflection by 0.5 mm in each step. The load-midspan deflection curves are shown in Figure 3. The overall shape of the curve, peak load and the corresponding displacement from the XFEM simulation using the bilinear law (figure inset) agrees very well with the experiment (thin curve). The effect of large deformation has been ignored in the present simulation, which may be significant at the final stage. If this effect is taken into account, the agreement may be further improved.

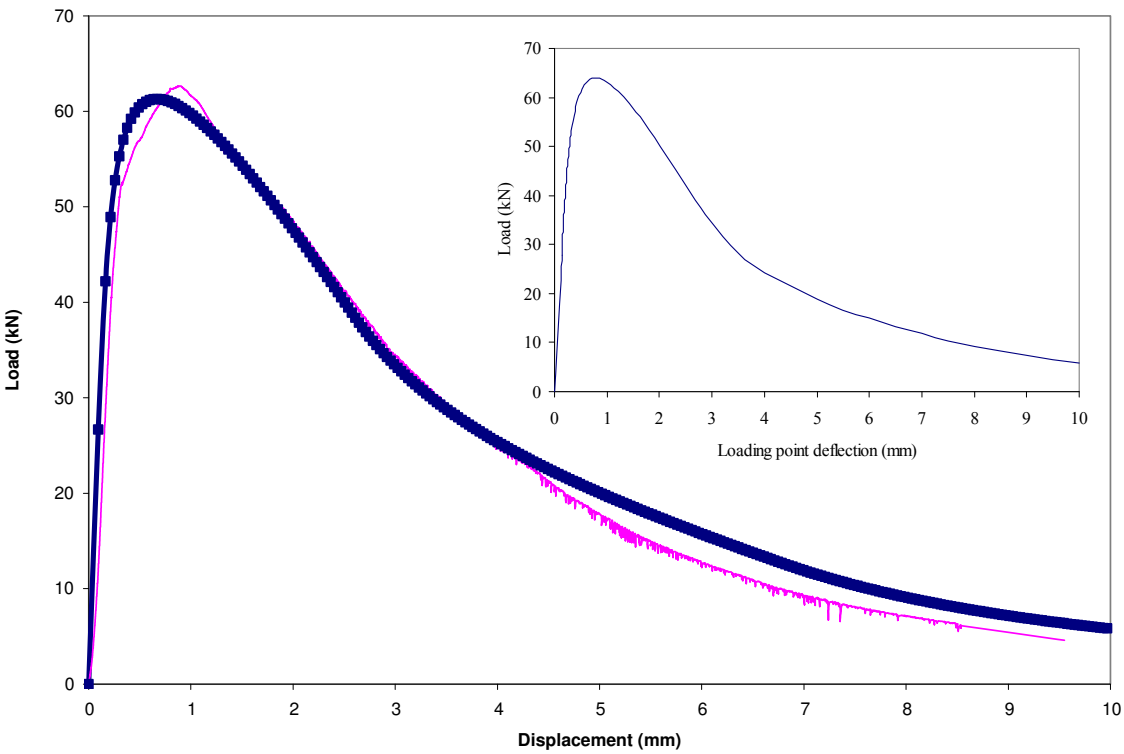

Figure 3. Large graph: load-deflection curves from experiments (thin curve) compared with an approximate method (thick curve/squares) in which the cohesive zone is regarded as a "hinge" in the central plane. Inset: load-deflection curve from the XFEM simulation. The agreement with the experimental curve is excellent both in terms of the shape and the maximum load carrying capacity.

References

[Babuška et al. 2003] I. Babuška, U. Banerjee, and J. E. Osborn, "Survey of meshless and generalized finite element methods: a unified approach", *Acta Numer.* **12** (2003), 1–125.

[Benson and Karihaloo 2005] S. D. P. Benson and B. L. Karihaloo, "CARDIFRC^{TM} - Development and mechanical properties, III: uniaxial tensile response and other mechanical properties", *Mag. Concrete Res.* **57**:8 (2005), 433–443.

[Borst et al. 2004] R. Borst, M. G. Gutierrez, G. N. Wells, J. J. C. Remmers, and H. Askes, "Cohesive-zone models, higher-order continuum theories and reliability methods for computational failure analysis", *Int. J. Numer. Methods Eng.* **60**:1 (2004), 289–315.

[Cornelissen et al. 1986] H. A. W. Cornelissen, D. A. Hordijk, and H. W. Reinhardt, "Experimental determination of crack softening characteristics of normalweight and lightweight concrete", *Heron* **31**:2 (1986), 45–56.

[Dugdale 1960] D. S. Dugdale, "Yielding of steel sheets containing slits", *J. Mech. Phys. Solids* **8**:2 (1960), 100–104.

[Hansbo and Hansbo 2004] A. Hansbo and P. Hansbo, "A finite element method for the simulation of strong and weak discontinuities in solid mechanics", *Comput. Methods Appl. Mech. Eng.* **193**:33-35 (2004), 3523–3540.

[Hillerborg et al. 1976] A. Hillerborg, M. Modeer, and P. E. Petersson, "Analysis of crack formation and crack growth in concrete by means of fracture mechanics and finite elements", *Cement Concrete Res.* **6**:6 (1976), 773–781.

[Karihaloo 1995] B. L. Karihaloo, *Fracture mechanics and structural concrete*, Longman, Harlow, Essex, 1995.

[Karihaloo and Xiao 2003] B. L. Karihaloo and Q. Z. Xiao, "Modelling of stationary and growing cracks in FE framework without remeshing: a state-of-the-art review", *Comput. Struct.* **81**:3 (2003), 119–129.

[Karihaloo and Xiao 2008] B. L. Karihaloo and Q. Z. Xiao, "Asymptotic fields at the tip of a cohesive crack", *Int. J. Fract.* **150** (2008), 55–74.

[Karihaloo and Xiao 2010] B. L. Karihaloo and Q. Z. Xiao, "Asymptotic fields ahead of mixed mode frictional cohesive cracks", *ZAMM Z. Angew. Math. Mech.* **90**:9 (2010), 710–720.

[Liu et al. 2004] X. Y. Liu, Q. Z. Xiao, and B. L. Karihaloo, "XFEM for direct evaluation of mixed mode SIFs in homogeneous and bimaterials", *Int. J. Numer. Methods Eng.* **59**:8 (2004), 1103–1118.

[Moës and Belytschko 2002] N. Moës and T. Belytschko, "Extended finite element method for cohesive crack growth", *Eng. Fract. Mech.* **69**:7 (2002), 813–833.

[Moës et al. 1999] N. Moës, J. Dolbow, and T. Belytschko, "A finite element method for crack growth without remeshing", *Int. J. Numer. Methods Eng.* **46**:1 (1999), 131–150.

[Strouboulis et al. 2001] T. Strouboulis, K. Copps, and I. Babuška, "The generalized finite element method", *Comput. Methods Appl. Mech. Eng.* **190**:32-33 (2001), 4081–4193.

[Wells and Sluys 2001] G. N. Wells and L. J. Sluys, "A new method for modelling cohesive cracks using finite elements", *Int. J. Numer. Methods Eng.* **50**:12 (2001), 2667–2682.

[Xiao and Karihaloo 2006a] Q. Z. Xiao and B. Karihaloo, "Asymptotic fields at frictionless and frictional cohesive crack tips in quasibrittle materials", *J. Mech. Mater. Struct.* **1**:5 (2006), 881–910.

[Xiao and Karihaloo 2006b] Q. Z. Xiao and B. L. Karihaloo, "Improving the accuracy of XFEM crack tip fields using higher order quadrature and statically admissible stress recovery", *Int. J. Numer. Methods Eng.* **66**:9 (2006), 1378–1410.

[Xiao et al. 2007] Q. Z. Xiao, B. L. Karihaloo, and X. Y. Liu, "Incremental-secant modulus iteration scheme and stress recovery for simulating cracking process in quasi-brittle materials using XFEM", *Int. J. Numer. Methods Eng.* **69**:12 (2007), 2606–2635.

[Zi and Belytschko 2003] G. Zi and T. Belytschko, "New crack-tip elements for XFEM and applications to cohesive cracks", *Int. J. Numer. Methods Eng.* **57**:15 (2003), 2221–2240.

Received 28 May 2010. Revised 27 Aug 2010. Accepted 8 Sep 2010.

BHUSHAN LAL KARIHALOO: karihaloob@cardiff.ac.uk
School of Engineering, Cardiff University, Cardiff, CF24 3AA, United Kingdom

QI-ZHI XIAO: qizhi.xiao@lusas.com
LUSAS FEA Ltd, Forge House, 66 High Street, Kingston-upon-Thames, KT1 1HN, United Kingdom